https://doi.org/10.5194/hess-2021-338
Preprint. Discussion started: 2 August 2021

Hydrology and Earth System Sciences
Discussions

Reactive Transport Modeling for Supporting Climate Resilience at Groundwater Contamination Sites

Zexuan Xu[1,*], Rebecca Serata[1], Haruko Wainwright[1], Miles Denham[2], Sergi Molins[1], Hansell Gonzalez-Raymat[4], Konstantin Lipnikov[3], David Moulton[3], Carol Eddy-Dilek[4]

1. Lawrence Berkeley National Laboratory;
2. Panoramic Environmental Consulting;
3. Los Alamos National Laboratory;
4. Savannah River National Laboratory

*Corresponding author: Zexuan Xu, zexuanxu@lbl.gov

ABSTRACT

Climate resilience is an emerging issue at contaminated sites and hazardous waste sites, since projected climate shifts (e.g., increased/decreased precipitation) and extreme events (e.g., flooding, drought) could affect ongoing remediation or closure strategies. In this study, we develop a reactive transport model (Amanzi) for radionuclides (uranium, tritium, and others) and evaluate how different scenarios under climate change will influence the contaminant plume conditions and groundwater well concentrations. We demonstrate our approach using a two-dimensional reactive transport model for the Savannah River Site F-Area, including mineral reaction and sorption processes. Different recharge scenarios are considered by perturbing the infiltration rate from the base case, as well as considering cap failure and climate projection scenarios. We also evaluate the uranium and nitrate concentration ratios between scenarios and the base case to isolate the sorption effects with changing recharge rates. The modeling results indicate that the competing effects of dilution and remobilization significantly influence pH, thus changing the sorption of uranium. At the maximum concentration on the breakthrough curve, higher aqueous uranium concentration implies that sorption is reduced with lower pH due to remobilization. To better evaluate the climate change impacts in the future, we develop the workflow to include the downscaled CMIP5 (Coupled Model Intercomparison Project) climate projection data in the reactive transport model, and evaluate how residual contamination evolves through 2100 under four climate Representative Concentration Pathway (RCP) scenarios. The integration of climate modeling data and hydro-geochemistry models enables us to quantify the climate change impacts, assess which impacts need to be planned for, and therefore assist climate resiliency efforts and help guide site management.

1. INTRODUCTION

Changing climate may cause unknown risk and uncertainty in environmental remediation, particularly in regard to the fate, transport, including both hydrologic and reactive processes (Maco et al., 2018). In particular, many sites are managed with monitored natural attenuation

https://doi.org/10.5194/hess-2021-338
Preprint. Discussion started: 2 August 2021


Hydrology and Earth System Sciences
Discussions

strategies where a significant amount of residual contaminants remain in the subsurface (Denham et al., 2020). Hydrological shift is one of the principal causes of this uncertainty and therefore also the risk. As climate change evolves, precipitation and evapotranspiration may change both in magnitude and timing, significantly affecting infiltration. Precipitation regimes are expected to change depending on where the site is located (e.g., Lambert et al., 2008). Increasing evapotranspiration is usually predicted in climate model projection, due to increasing temperatures under global warming (e.g., Abtew and Melesse, 2013, Milly and Dunne, 2016). Extreme climatic events, such as flooding and droughts, are expected to become more frequent and thus may result in faster plume remobilization (e.g., Rahmstorf and Coumou, 2011).

We may define climate resilience at contaminated sites as the capacity of individual waste disposal sites to absorb the projected stresses imposed by climate trends, climate variability, extreme events, and other climate-change-related impacts. The researches that addressed climate change impacts on groundwater contamination and nuclear waste remediation are limited, although a critical need exists due to the changing climate. Most of the previous studies (e.g., Gellens and Roulin, 1998; Green et al., 2011; Middelkoop et al., 2001; Pfister et al., 2004) focuses on evaluating the effect of climate change on the abundance of water resources, water quality and contamination issues were less investigated (Visser et al., 2012). Within those studies, most previous studies focuses on surface water (Wilby et al., 2006; Van Vliet and Zwolsman, 2008; Van Bokhoven, 2006; Futter et al., 2009; Schiedek et al., 2007), because of the accessibility and data availability (Green et al., 2011). For groundwater in the subsurface domain, most studies evaluate agricultural effluents at the regional scale (Bloomfield et al., 2006; Futter et al., 2009; Li and Merchant, 2013; Olesen et al., 2007; Sjoeng et al., 2009; Whitehead et al., 2009; Wilby et al., 2006; Darracq et al., 2005; Destouni and Darracq, 2009; Park et al., 2010).

Recently, Libera et al. (2019) investigated the potential impacts of climate change on residual contaminants in vadose zones and groundwater, using a groundwater flow and transport model. They investigated the complex effect of precipitation and recharge shifts, leading to either dilution and remobilization of residual contaminants. Libera et al (2019) showed that the effects of dilution and remobilization on contaminant concentrations appear in different phases, depending on the well locations, and that surface barrier and source zone monitoring are critical for mitigating the impact. However, Libera et al. (2019) only simulated tritium, which is a nonreactive contaminant. Large uncertainties still remain, particularly for reactive contaminants, due to complex geochemical processes in the subsurface. The impact of hydrological shifts on reactive contaminants is expected to be more complex, especially redox and pH-sensitive heavy metals. Remobilization would also be affected by additional clean infiltration water. To test those hypotheses and evaluate the impacts, process-based flow and reactive transport models that can characterize sorption and ion exchange processes are essential for quantitatively analyzing the contaminant plume and understanding climate resilience.

This study aims to evaluate the impacts of climate change-driven hydrological shifts on (1) reactive contaminants and (2) mineral reactions in vadose zones and groundwater. We used a numerical reactive transport model to study groundwater flow, contaminant transport, and

https://doi.org/10.5194/hess-2021-338
Preprint. Discussion started: 2 August 2021


Hydrology and Earth System Sciences
Discussions

mineral reactions with sorption in both vadose and saturated domains. The effects of changing precipitation are assumed to be represented by changing of natural recharge from surface through the aquifer system. The model is developed and applied at the Department of Energy (DOE)'s Savannah River Site (SRS) F-Area Seepage Basins, South Carolina (SC), USA, where various metals and radioactive contaminants exist in the soil and groundwater since 1950s. This is the same site studied by Libera et al. (2019). With extensive geophysical data for subsurface characterization and comprehensive groundwater chemistry and water level datasets at the SRS F-Area, the development of a subsurface model can be considered as a testbed for flow and transport studies (Flach, 2004; Bea et al., 2013; Sassen et al., 2012; Wainwright et al., 2014, 2015, 2016; Denham and Eddy-Dilek, 2017; Libera et al., 2019). Hence, the SRS has become a unique study site for investigating the potential consequences of a changing climate on contamination remobilization and mineral reactions/interactions.

2. SITE DESCRIPTION

The Savannah River Site F-Area in South Carolina is approximately 161 km (i.e., 100 mi) away from the Atlantic Ocean with an area of about 800 km^2 (Figure 1). Special radioactive isotopes, plutonium, and tritium were produced at this site for nuclear weapons during the Cold War Era. The F-Area is located in the north-central part of SRS. There are three hydrostratigraphic units within the Upper Three Runs Aquifer, shown in Figure 1 (B): an Upper Aquifer zone (UUTRA), a Tan Clay Confining Zone (TCCZ), and a Lower Aquifer zone (LUTRA). The UUTRA and LUTRA are primarily composed of clean sand with relatively high permeability, while the TCCZ is a low-permeability layer with mixed sand-and-clay. The UUTRA and LUTRA units are hydrologically connected based on the piezometric head measurements. A competent clay layer confining unit at the bottom of LUTRA, namely, the continuous Gordon Confining Unit, at the bottom of LUTRA, separates the deeper aquifer (Gordon Aquifer) from the upper two aquifer units (Figure 1). The historical monitoring data collected at F-Area have shown that the contaminant plume migrates between the UUTRA and LUTRA (Figure 2), discharging into a local stream called Fourmile Branch.

Low-level radioactive acidic waste was disposed of in three separate unlined seepage basins (F-1, F-2, and F-3) and leached into the groundwater. During 1955 to 1988, the basins received approximately 7.1 billion liters of waste solutions due to uranium industry. The F-Area basins were closed and capped with a low-permeability material in 1988 after discharge operations ended. At present, an contaminant plume with low pH and high uranium concentration extends downgradient from the basins approximately 600 m to the groundwater seepage area near the Fourmile Branch Creek. Several measures have been taken to reduce the environmental impacts at the F-Area site, including capping the basins and pump-and-treat remediation of contaminated groundwater. In 2004, a funnel-and-gate system with groundwater flow barriers were constructed to decrease the groundwater gradient and enhance natural attenuation. Also base injection were used to neutralize pH and in turn immobilize uranium. Although many active remediation have been applied in the past several decades, the groundwater remains

https://doi.org/10.5194/hess-2021-338
Preprint. Discussion started: 2 August 2021


Hydrology and Earth System Sciences
Discussions

unnaturally acidic with high level of various radionuclides and other contaminants in the upgradient of the funnel-and-gate (Seaman et al., 2007, Savannah River Nuclear Solution, 2021).

The main characteristic of the SRS F-Area is the high acidity of the plume, which makes U(VI) highly mobile. The natural groundwater pH is slightly acidic, between 5.0 and 6.0, and decreases to values approaching 3.2 in the most contaminated locations. It should be noted that in the acidic pH range at the SRS-F-Area, Kd values for U(VI) can vary between 10^2 to 10^6 (Davis et al., 2004; Dong et al., 2012). In addition, competing sorption between U(VI) and H^+ is important in remediation and well studied in the F-Area site (Davis et al., 2004, Bea et al., 2013, Arora et al., 2018). Due to the complex geochemical conditions in groundwater and mobility of U(VI), uncertainty quantification (UQ) related to U(VI) and H^+ competing sorption have been performed in the F-Area site in the previous studies (e.g., Curtis et al., 2006; Hammond et al., 2011). Our research focuses on the effect of climate change on progress toward return to natural conditions of the acidic portion of the plume between the basins and the funnel-and-gate. This is important to the timing of the transition of the site from enhanced to monitored natural attenuation, and hence, important to the overall effectiveness of remediation. More importantly, this work will contribute to the remediation of the site and support the risk management under changing climate conditions.

https://doi.org/10.5194/hess-2021-338
Preprint. Discussion started: 2 August 2021

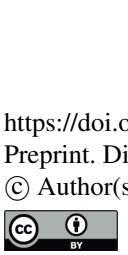

Hydrology and Earth System Sciences
Discussions
Open Access
EGU

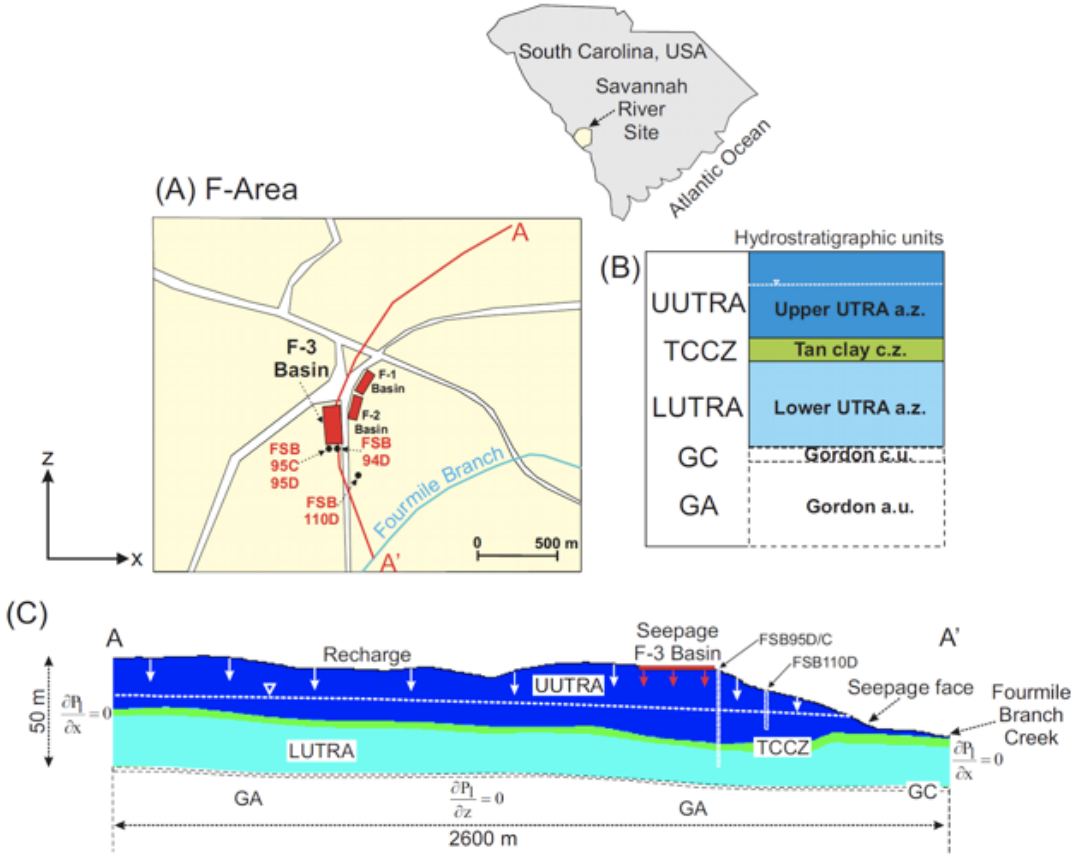

170 Figure 1. (A) Location of seepage basins in the F-Area of the Savannah River Site (SRS); (B) Hydrostratigraphic units defined for the F-Area; (C) 2D-cross section model domain. Modified from Bea et al. (2013).

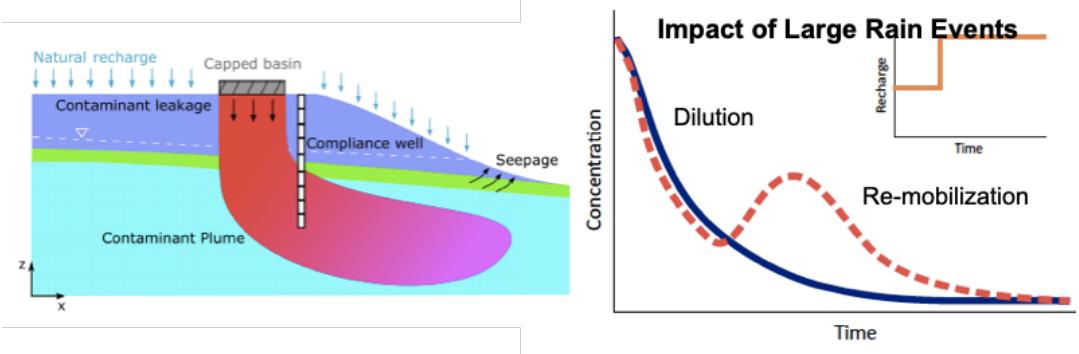

175 Figure 2. Left) Schematic figure of the two-dimensional cross section hydrological conceptual model, representing the middle line of the contaminant source zone; Right) Schematic diagram

https://doi.org/10.5194/hess-2021-338
Preprint. Discussion started: 2 August 2021


Hydrology and Earth System Sciences
Discussions

showing the concentration breakthrough curve (BTC) at a downgradient observational well with increasing recharge rate. Modified from Libera et al. (2019).

3. MODELING METHODS

3.1. Reactive Transport Modeling with Amanzi and PFLOTRAN

Groundwater flow and contaminant transport are simulated by the numerical code Amanzi (Moulton et al., 2013, https://github.com/amanzi/amanzi), which provides a flexible and extendable parallel flow and reactive transport simulation capability for environmental applications. Amanzi has the capabilities to solve coupled unsaturated and saturated groundwater flow, as well as advection-dispersion transport equations. It includes a general polyhedral mesh infrastructure, and provides multiple advanced nonlinear solvers with open source libraries. The reaction of contaminants and minerals carried by flow through the surrounding rock and soil is modeled by coupling with the geochemistry engine of PFLOTRAN (Lichtner et al., 2015) or CrunchFlow via the generic interface Alquimia (Johnson and Molins, 2015, https://github.com/LBL-EESA/alquimia-dev). PFLOTRAN or CrunchFlow simulates the mineral reactions, adsorption, and ion exchange, while groundwater flow and transport are simulated by Amanzi.

3.2. Model Setup and Boundary Conditions

The two-dimensional (2D) flow and transport model developed in Libera et al. (2019) was employed in this study, while the geochemistry database, mineral composition and kinetic reaction were implemented based on a previous study by Bea et al. (2013). The 2D domain is along the groundwater flow line in the F-Area, with approximately 2600 m long and 100 m deep. Bea et al. (2013) calibrated the model and verified it using observational geochemical concentration data from several monitoring wells, and also evaluated the sensitivities of key parameters in the modeling. The vadose zone and three hydrostratigraphic units (i.e., UUTRA, LUTRA, and TCCZ) defined in the previous section are included in the model. Hydrogeological properties are assumed homogeneous within each unit (see Table 2), based on site investigation reports and previous studies. The hydrological parameters, including specifies porosity, permeability, and capillary pressure/saturation data, are listed in Table 1 (Flach et al., 2004; Bea et al., 2013). The system is considered to be advection dominated; therefore, mechanical dispersion and molecular diffusion transport processes are neglected.

TABLE I. Physical model parameters used in the simulations. α, n and Θr are the parameters of inverse air entry suction, a measure of the pore-size distribution, and residual water content, respectively, in the van Genuchten water retention curve.

Hydrostratigraphic unit	Porosity [-]	Permeability [m^2]	α [-]	n [-]	Θr [-]

https://doi.org/10.5194/hess-2021-338
Preprint. Discussion started: 2 August 2021

Hydrology and Earth System Sciences
Discussions

Upper aquifer (UUTRA)	0.39	5e-12	4e-4	1.37	0.18
Tan clay (TCCZ)	0.39	1.98e-14	5.1e-5	2	0.39
Lower aquifer (LUTRA)	0.39	5e-12	5.1e-5	2	0.41

No-flow boundary conditions are assigned along the two vertical sides of the 2D-cross section (see Figure 2) according to the groundwater divides, modified from previous studies (Flach, 2004; Bea et al., 2013). The confining at the bottom of the computational domain is highly clay-rich, therefore, no-flow boundary condition is set at the bottom of the computational domain (Bea et al., 2013). The geochemical initial and boundary conditions in Table 2 are set to be the same as Bea et al. (2013), with a small modification of the nitrate-concentration initial condition for better matching with the observation. Based on previous studies and field investigations, eight minerals are simulated in the reactive transport model in the F-Area. Table 3 below listed the kinetic rate of the primary minerals (i.e., quartz, kaolinite, and goethite) simulated in the model. In addition, gibbsite, jurbanite, basaluminite, opal, and schoepite minerals are included as they may form when the plume interacts with the solids.

TABLE 2. Chemical composition for the background (initial), recharge and seepage solutions (modified from Bea et al., 2013). Unit is mol kgw^{-1}, except pH and CO_2 (aq).

Mineral	Background and Recharge	Seepage
pH	5.4	1.54
Al^{3+}	2.21e-8	1.00e-8
Ca^{2+}	1.00e-5	1.00e-5
Cl^-	9.98e-3 [a]	3.39e-4
Fe^{3+}	2.92e-16 [b]	2.75e-6
CO_2 (g)	$10^{-3.5}$ [c]	$10^{-3.5}$ [c]
K^+	3.32e-5	1.72e-6
Mg^{2+}	5.35e-3	2.47e-5
Na^+	2.78e-4	6.82e-5
SiO_2 (aq)	1.77e-4	1.18e-4
SO_4^{2-}	2.25e-5	4.80e-5
Tritium	1.0e-15	2.17e-9
NO_3^-	1.0e-4	1.00e-2
UO_2^{2+}	1.25e-10	3.01e-5

https://doi.org/10.5194/hess-2021-338
Preprint. Discussion started: 2 August 2021

Hydrology and Earth System Sciences
Discussions

a: Calculated as electric charge balance; b: Equilibrium with Kaolinite; c: fixed by atmosphere pressure of

TABLE 3. Initial mineral volumetric fraction distribution in the simulation (Bea et al., 2013).

Mineral	wt.% [-]	Vol. frac. [-]	Surface area [m^2 g^{-1}]	Density [g cm^{-3}]
Quartz	94.5	0.9496	0.14	2.648
Kaolinite	4.015	0.0412	20.71	2.594
Goethite	1.485	0.0093	16.22	4.268
Schoepite	0	0	0.1	4.874
Gibbsite	0	0	0.1	2.44
Basaluminite	0	0	0.1	2.119
Opal	0	0	0.1	2.072
Jurbanite	0	0	0.1	1.789

While Bea et al. (2013) implemented an electrostatic sorption model developed previously by Dong et al. (2012), which is less numerically efficient and requires additional parameterization. Arora et al. (2018) developed a non-electrostatic sorption model (NEM) at the F-Area site, and demonstrated that NEM achieved the same predictive performance as a surface complexation model (SCM) with electrostatic correction terms. The SCM approach is computationally expensive and requires the estimation of additional parameters that describe mineral surface characteristics. On the other hand, NEM does not consider the effects of the development of surface charge on the formation of surface complexes, and it also simplifies the parameters needed in the reactive transport modeling. In Arora et al. (2018), three mineral surface sites with different site densities and acidity constants are developed for modeling H^+ sorption and transport, then further extended to noncompetitive and competitive H^+ and U(VI) sorption in a one-dimensional test case. In this paper, we use the competitive H^+ and U(VI) sorption NEM parameters (including site density and surface complexation constant listed in Table 4), which are derived from an inverse analysis and calibration by Arora et al. (2018), and implement them in the model.

TABLE 4. NEM model parameters for H^+ and U(VI) competitive sorption (Arora et al., 2018).

Site	Site density (moles/m^2)
>TOH	7.0e-7
>XOH	1.6e-6
>YOH	9.0e-7
Reactions	Surface Complexation Log K

https://doi.org/10.5194/hess-2021-338
Preprint. Discussion started: 2 August 2021


Hydrology and Earth System Sciences
Discussions

$>TOH_2^+$ --- $>TOH + H^+$	-4.77
$>TO^-$ --- $>TOH^- + H^+$	4.73
$>XOUO_2^+$ --- $>XOH + UO_2^{2+} - H^+$	-0.67
$>YOH_2^+$ --- $>YOH + H^+$	-3.41

3.3. CMIP5 Climate Scenarios

CMIP5 (Coupled Model Intercomparison Project, Taylor et al. (2012) is an experimental protocol with an ensemble of global climate model outputs to improve understanding of climate, and to provide estimates of future climate change that will be useful to those considering its possible consequences. The climate forcing in our study used the 1/8-degree downscaled CMIP5 outputs at the F-Area study site from January 1950 to December 2100. The ensemble outputs include 28 models with four climate scenarios (RCP2.6, 4.5, 6.0 and 8.5) in the future climate projection. The top soil at the F-Area study site is sandy (Wainwright et al., 2014), so we assume that surface runoff is negligible. In other words, infiltration is calculated by subtracting evapotranspiration from precipitation, which are simulated by the atmospheric and land surface models, respectively, from the coupled climate models. The figure below shows that the 10-year moving average of selected variables demonstrates that both precipitation and evapotranspiration have increased approximately 6% since the 1950s to the present, and will keep increasing up to an additional 6% by the end of this century. The differences among climate scenarios are not statistically significant, but the highest greenhouse gas concentrations (i.e., RCP8.5) ensemble simulates higher precipitation and evapotranspiration than others. Although both precipitation and evapotranspiration are increasing (hence the difference is offset), the total runoff still slightly increases, with significant variability among climate scenarios over time (Figure 3).

https://doi.org/10.5194/hess-2021-338
Preprint. Discussion started: 2 August 2021

Hydrology and Earth System Sciences
Discussions

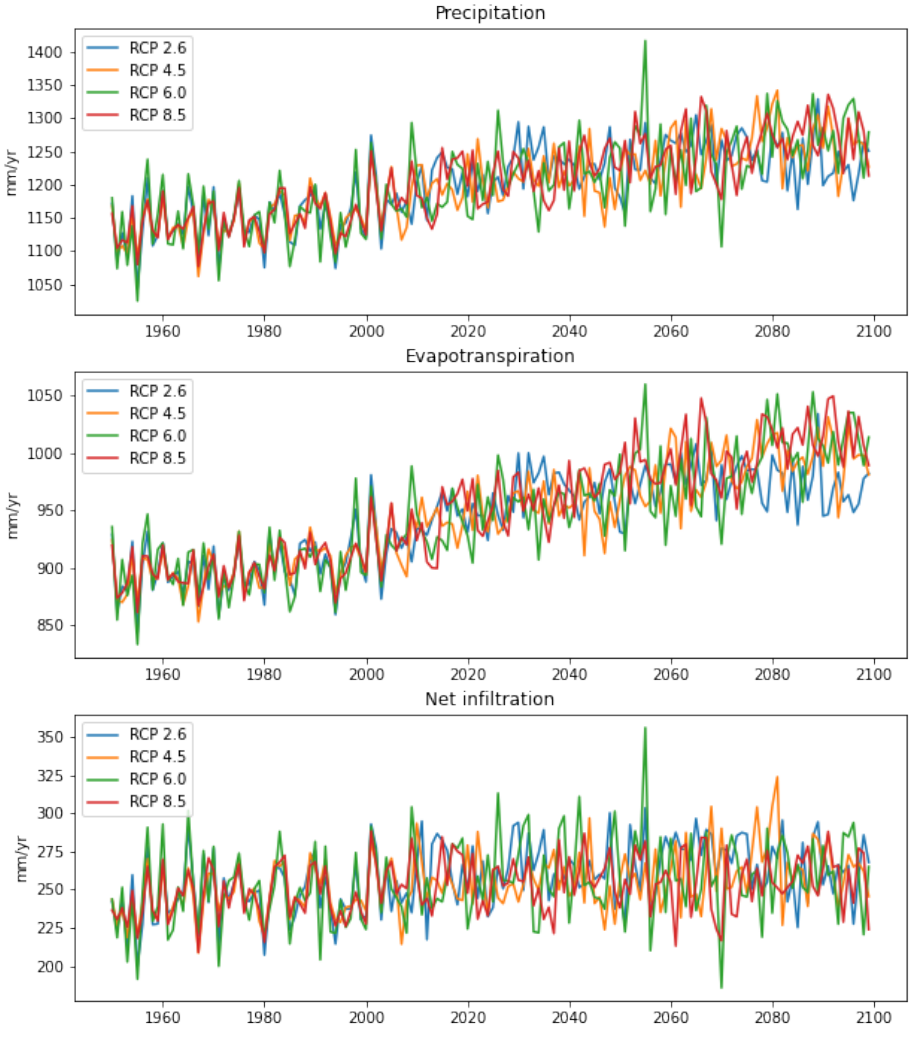

270 Figure 3. Simulated precipitation, evapotranspiration, and net infiltration (precipitation - evapotranspiration) at different climate projection scenarios from the CMIP5 datasets.

https://doi.org/10.5194/hess-2021-338
Preprint. Discussion started: 2 August 2021


Hydrology and Earth System Sciences
Discussions

3.4. Modeling Scenarios

The modeling scenarios were developed based on (Libera et al., 2019) are only briefly described here. The modeling scenarios cover two stages of the F-Area historical operation and one additional stage in the future projection. The waste disposal was active during the period 1955-1988, and the basins were capped in 1988, when seepage from the basins into the vadose zone was halted. This study evaluates climate change impact with changing recharge on contaminant transport after 2020. A base case was developed with a constant recharge rate throughout the simulation period for assessing climate change impacts. The uniform recharge rate is 4.743e-06 kg-water/m^2/sec (0.15 m/yr infiltration rate), based on the estimation in Bea et al. (2013). Furthermore, we developed three scenarios, with perturbation with respect to the baseline recharge conditions. The three scenarios are: (1) constant positive recharge shift from 2020, i.e., increasing precipitation scenarios; (2) constant negative recharge shift from 2020, i.e., decreasing precipitation scenarios; and (3) cap failure and constant positive case from 2020. In both increasing and decreasing scenarios, recharge changes 10%-50% after 2020. In the cap failure scenarios, an increased recharge of 10%-50% is added to the level of the to represent a complete failure of the containment structure at the source-zone region. In addition to the perturbation scenarios, the contaminant transport and plume remobilization simulated by Amanzi are also forced by the four projection scenarios of CMIP5 ensemble climate model data, i.e., climate model scenarios. Instead of the constant recharge rate in Stage I and II in all perturbation cases and Stage III in the base case, the annual recharge rate is computed by the difference between precipitation and evapotranspiration in the CMIP5 data from 1950 to 2100.

4. RESULTS

4.1. Base Case

The plume migration is depicted in Figure 4 for the base-case results described in Bea et al. (2013). The plume migrates through the vadose zone and then infiltrates vertically downward until it reaches the groundwater table (Figure 4a). The plume then migrates vertically through the TCCZ into the LUTRA, and also horizontally downstream closer to the FMB Creek (Figure 4b). Despite the relatively low permeability of the TCCZ, flow from the UUTRA to the LUTRA is observed over most of the domain. After basin closure and capping, the seepage from the basin is assumed to stop. The uncontaminated groundwater arriving from upgradient increased pH and reduced the U(VI) concentration (Figure 4c). After the basin closure, because the vadose zone flow stops, pH remains acidic and U(VI) concentrations high in the vadose zone. In addition, the uranium concentration is higher in the TCCZ, where the permeability is low. The vadose zone below the basin appears to act as a long-term contaminant source for groundwater in the deeper layers (Figure 4d). Although aqueous uranium concentration decreased by several orders of magnitude after the basin was capped, it is still higher than background concentration.

https://doi.org/10.5194/hess-2021-338
Preprint. Discussion started: 2 August 2021

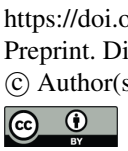

Hydrology and Earth System Sciences
Discussions

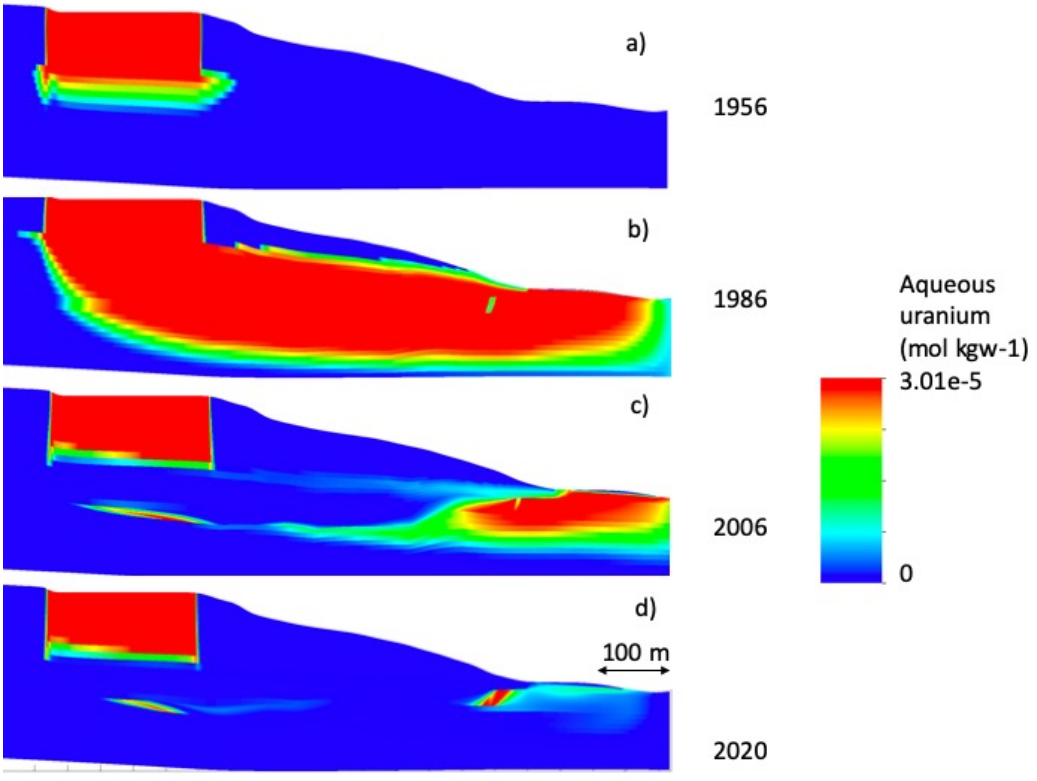

Figure 4. Plume profile of aqueous uranium concentration in the downstream of F-Area study site from 1954 to 2020 in the base case simulation.

Figure 5 shows the base-case breakthrough curves of pH, aqueous uranium, tritium, and nitrate at the source-zone well (FSB-95DR) and the downgradient well (FSB-110D) for the full simulation period (1956-2100). Both wells are located in the UUTRA layer. The simulated pH values rapidly decrease to 3.3 at both the source-zone well (Figure 5a) and the downgradient well (Figure 5c). In general, tritium concentrations (Figure 5c) decrease faster and more dramatically than aqueous uranium and nitrate, owing to its radioactive decay. The uranium concentrations (Figure 5b) increased from the background level 1.25e-10 mol kgw^{-1} to 3.0e-5 mol kgw^{-1} at both wells in less than a few years, and remained constant until basin closure in 1988. After the basin closure, pH rebounds to 4.0 in 2000 and gradually increases throughout the end of simulation. Similarly, uranium concentration (Figure 5b) decreases by two orders of magnitude in 20 years and keeps decreasing to approximately 1.0e-7 mol kgw^{-1} by the end of the simulation period. Compared to the downgradient well, the source-zone well consistently has lower pH (Figure 5a) and higher aqueous uranium (Figure 5c) concentrations throughout the simulation period. By the end of 2100, pH (Figure 5a) is higher than 5.0 and aqueous uranium concentration lower than 2e-7 mol kgw^{-1} (Figure 5b) in most of the vadose zone at the source-zone well.

https://doi.org/10.5194/hess-2021-338
Preprint. Discussion started: 2 August 2021

Hydrology and Earth System Sciences
Discussions

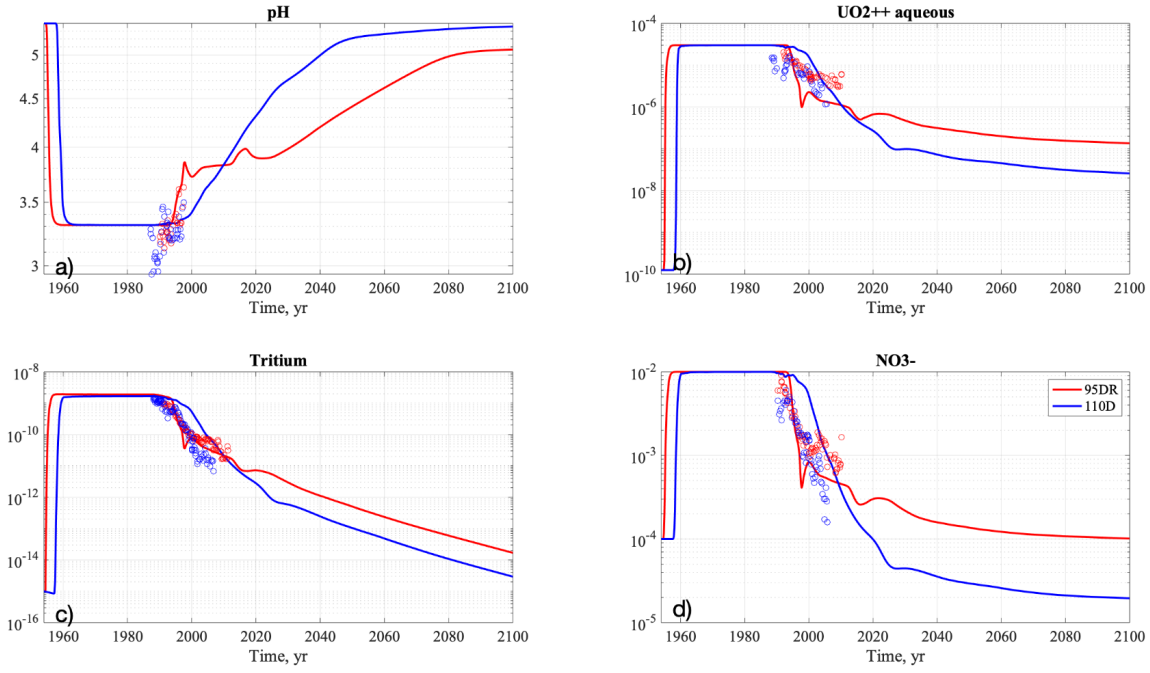

335 Figure 5. Breakthrough curves of pH, aqueous uranium, tritium and nitrate at the source-zone well and downgradient well in the base case over the simulation period (1954-2100).

4.2. Increasing Recharge Scenarios

The breakthrough curves under the increasing recharge scenarios are shown in Figure 6. When
340 recharge is increased, pH at the source-zone well (Figure 6a) is significantly lower compared to the base-case scenario. pH values are changed with different recharge rates as relatively high pH infiltrated rainwater dilutes the low-pH contaminated environment in the subsurface system. However, the relationship between recharge and pH is nonlinear, with thresholds such that pH is the lowest at +20% recharge, while pH is higher in the cases with +30% to +50% recharge.
345 Nitrate concentrations at the source-zone well (Figure 6b) increase immediately after 2020, and spike 5 years after perturbation, with the highest concentration in the greater recharge (+50%) case. After 2050, nitrate concentration is the highest with +20% recharge, and decreases from +30% to +50% recharge (Figure 6b). The tritium concentrations (Figure 6c) peak similarly to nitrate, although tritium decreases significantly after 2040 due to radioactive decay. The
350 uranium concentrations (Figure 6d) are also similar to the breakthrough curves for the nitrate concentrations. At downgradient locations, pH (Figure 6e) is not influenced by the recharge increase up to +30%. Above the 40% increase, pH decreases significantly after 2040. Nitrate concentrations at the downgradient well (Figure 6f) decrease immediately after 2020 due to

https://doi.org/10.5194/hess-2021-338
Preprint. Discussion started: 2 August 2021

Hydrology and Earth System Sciences
Discussions

dilution, but increase afterwards, with peaks around 2040. Similar to the source-zone well (Figure 6b), the concentration peaks are higher with greater recharge rates and remain higher than the base case throughout the end of the simulations. The tritium concentrations (Figure 6g) keep decreasing after 2020 with the peaks in 2040, with the similar behavior of sudden increase showing in nitrate concentration (Figure 6f), and higher concentrations in the high recharge scenarios. The uranium concentrations (Figure 6h) also exhibit patterns similar to those of nitrate (Figure 6f), in that both the peak and remaining concentrations are higher in the greater recharge scenarios.

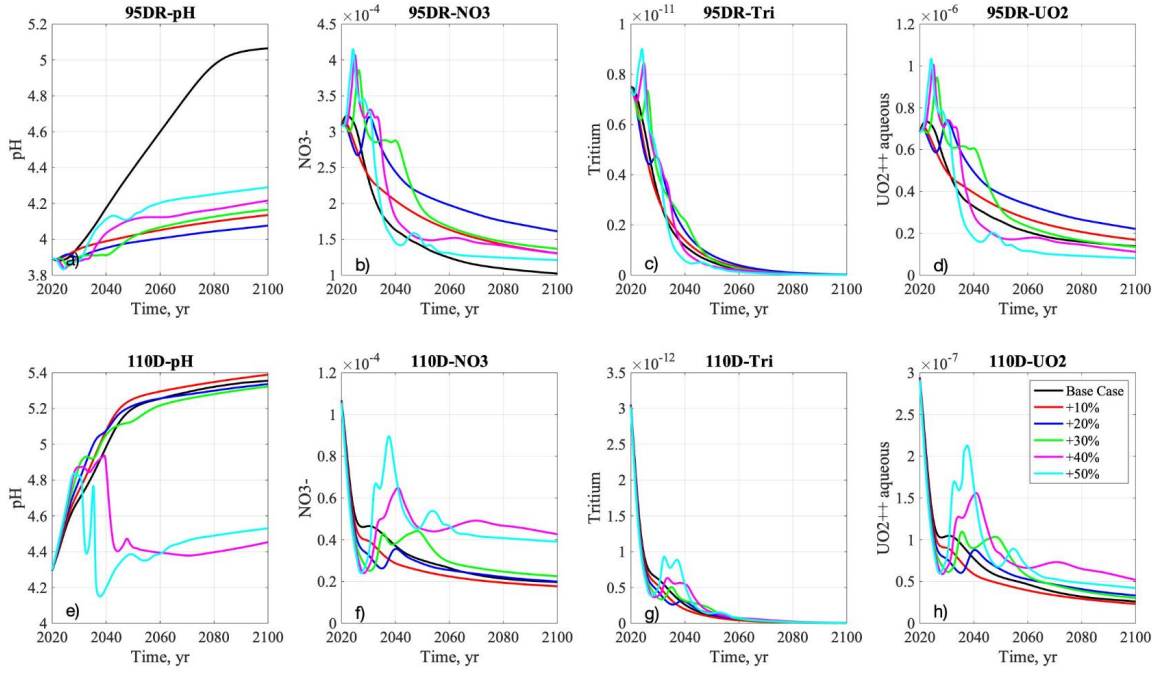

Figure 6: Breakthrough curves of pH, nitrate, tritium, and aqueous uranium at the source-zone well (a-d) and downgradient well (e-h) in the base case and increasing precipitation scenarios from 2020 to 2100.

The reactive (uranium) and non-reactive (nitrate) species are compared in Figure 7. Kd values are computed by sorbed uranium concentration in the solid phase with the aqueous uranium concentration from the model outputs. Figure 7a shows that Kd values at the source-zone well are lower in the increasing recharge cases than the base case, which is consistent with pH breakthrough curves (Figure 6a). The +20% case has the lowest Kd at the source-zone well, while the Kd values are higher in the smaller recharge case (+10%) and greater recharge cases beyond +30%. In contrast, at the downgradient well (Figure 7d), the Kd values are lower in the +40% to +50% scenarios echoing the downgradient pH breakthrough curves in Figure 6e. In addition, we compare uranium and nitrate concentrations with respect to the maximum

https://doi.org/10.5194/hess-2021-338
Preprint. Discussion started: 2 August 2021

Hydrology and Earth System Sciences
Discussions
Open Access
EGU

concentration (i.e., the peak concentrations that occur after a few years in the increasing recharge scenarios) as well as the average concentration from 2040 to 2100, which illustrates the long-term contamination trend. Figure 7 (b-c) presents the ratio of uranium and nitrate, defined as the concentration in each scenario compared to the baseline case. In the maximum concentration at the source-zone well (Figure 7b), the ratios are mostly higher than 1, demonstrating that the maximum concentration is higher in the greater increasing recharge scenarios. The uranium maximum concentration ratio is higher than the nitrate; therefore, the increasing recharge affects the uranium concentrations more than the nitrate concentrations at the peaks (Figure 7b). For average concentrations at the source-zone well (Figure 7c), the ratio increases in the +20% recharge case, but decreases at greater recharge values. Different from the maximum concentrations, the mean uranium ratio becomes lower than the mean nitrate ratio, and falls below 1.0 in the greater recharge scenarios (Figure 7c). At the downgradient well, the maximum concentration ratios are less than 1.0 in the (+10% ~ +30%) recharge scenarios but higher than the base case in greater recharge (+40~50%) scenarios, while nitrate and uranium ratios are similar (Figure 7e). The average concentration ratios at the downgradient well after 2040 are generally higher with increasing recharge, and reach their highest at the +40% scenario (Figure 7f). The nitrate concentration ratios are lower than uranium in the smaller (+10% ~ +30%) recharge scenarios, but are higher in those scenarios of above +40% recharge.

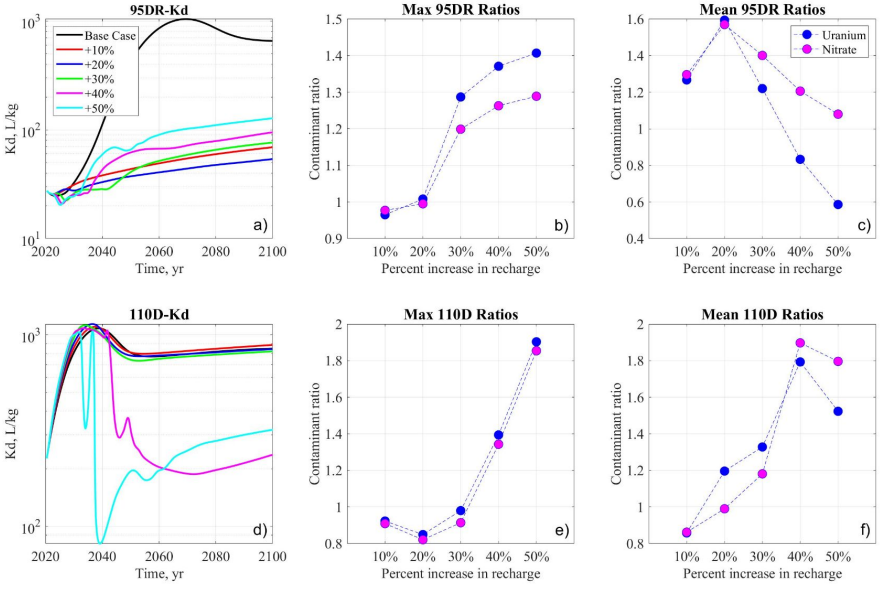

Figure 7 : Breakthrough curves for Kd at the source-zone well (a-c) and the downgradient well (d-f) for the increasing recharge scenario from 2020 to 2100. Maximum and average ratios of base case to increased recharge case for uranium and nitrate concentrations at both well locations.

https://doi.org/10.5194/hess-2021-338
Preprint. Discussion started: 2 August 2021


Hydrology and Earth System Sciences
Discussions

4.3. Decreasing Recharge Scenarios

Although decreasing recharge has little impact on pH at the source-zone well up to -30% (Figure 8), pH increases significantly in the -40% ~ -50% recharge scenarios. The nitrate concentrations (Figure 8b) increase immediately after the perturbation of recharge, then decrease throughout the end of the simulation. Similarly to pH, nitrate concentrations (Figure 8b) do not change significantly in smaller decreasing recharge scenarios, but decrease two orders of magnitude in the greater (-40 ~ -50%) decreasing recharge scenario. Tritium concentrations (Figure 8c) also increase immediately after 2020, then decrease; the rate of decrease is more rapid than the nitrate concentrations due to radioactive decay, and exhibit few differences among decreasing recharge scenarios. The uranium concentration (Figure 8d) breakthrough curves are similar to the nitrate curves. At the downgradient well, the pH values have a similar trend to the source-zone well in all decreasing recharge scenarios before 2040. However, the breakthrough curves diverge after 2040 and increase more in the greater decreasing recharge scenarios. The pH values are higher than the source-zone well and reach as high as 7.0 in the -50% recharge scenario in 2100 (Figure 8e). The nitrate concentrations in the down gradient well (Figure 8f) keep decreasing in the first 10-15 years after 2020. Concentrations peak around 2025-2035; the decrease is more significant in all the decreasing recharge scenarios than the base case. In general, the peak concentrations occur earlier and higher in the greater decreasing recharge scenarios, and the breakthrough curves decrease faster and lower in the long-term projection to 2100. Spikes were observed in the tritium concentration breakthrough curves (Figure 8g), as well as with smaller magnitudes at the down gradient well 10-15 years after the perturbation. The uranium-concentration breakthrough curves (Figure 8h) are similar to the nitrate concentrations, but decrease more rapidly in all cases.

https://doi.org/10.5194/hess-2021-338
Preprint. Discussion started: 2 August 2021

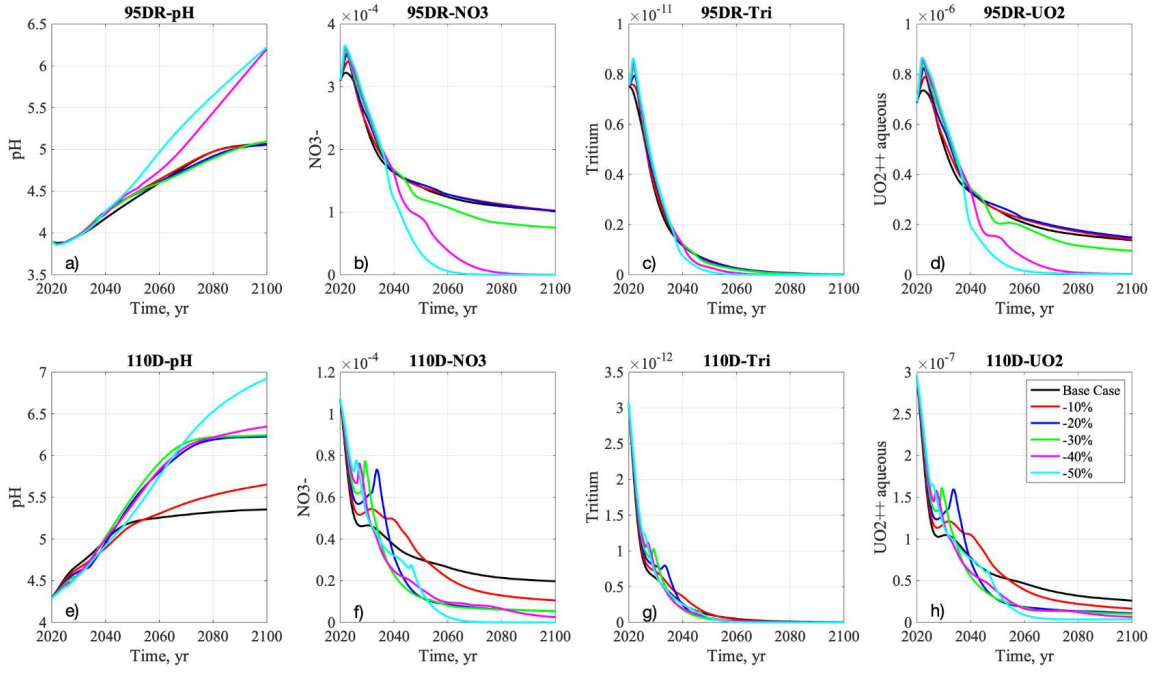

Figure 8: Breakthrough curves of pH, nitrate, tritium, and aqueous uranium at the source-zone well (a-d) and downgradient well (e-h) in the base case and decreasing precipitation scenarios from 2020 to 2100.

Kd breakthrough curves generally reflect the pH breakthrough curves in Figure 8 and are higher in the decreasing recharge scenarios at both well locations. Figure 9a shows that at the source-zone well, the base case ~ -30% cases have relatively similar Kd values throughout the simulation period. After 2060, the -40% and -50% recharge scenarios both significantly increase. At the downgradient, Kd values are generally higher than source-zone well, and the difference in Kd values among cases are more pronounced (Figure 9d). Kd value is the lowest in the higher recharge (base case and -10%) scenarios, and largest in the significantly decreasing recharge (-50%) case. The -10% and -20% recharge scenarios significantly diverge at 2040 and converge at 2100. Similar to the increasing recharge scenarios, maximum uranium and nitrate concentrations at the source-zone well occur immediately a few years after the perturbation (Figure 8). With decreasing recharge from -10% to -50%, maximum concentration ratios are higher than 1.0 and increase with decreasing recharge, while average concentration ratios are generally lower than 1.0. In Figure 9b, the uranium maximum concentration ratios are slightly higher than nitrate, with greater difference in the -50% recharge case. In Figure 9c, the ratios of long-term average concentrations show that both uranium and nitrate concentration are nearly the same as the base case in smaller decreasing recharge scenarios (-10% ~ -20%), but decrease quickly and are significantly lower in the greater decreasing recharge scenarios (-30% ~ -50%). Compared to the results at the source-zone well, the maximum and average

https://doi.org/10.5194/hess-2021-338
Preprint. Discussion started: 2 August 2021

Hydrology and Earth System Sciences
Discussions
Open Access
EGU

concentration ratios at the downgradient well (Figure 9e and f) have similar trends. Nitrate maximum concentration ratios are higher than nitrate (Figure 9e), and their differences are the greatest in the -20% and -30% recharge case. The average concentration ratios (Figure 9f) decrease with decreasing recharges, and uranium ratios are consistently higher than nitrate.

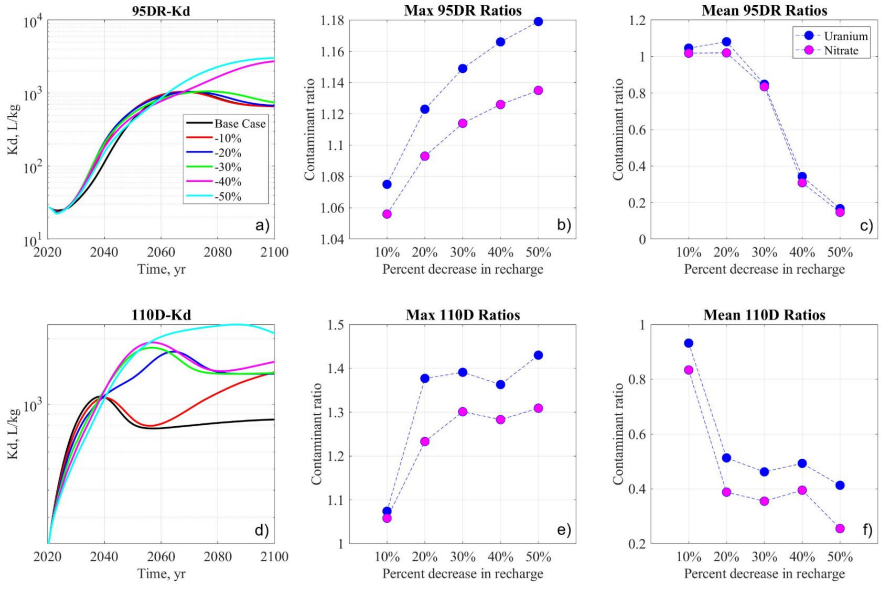

Figure 9 : Breakthrough curves for Kd at the source-zone well (a-c) and the downgradient well (d-f) for the increasing recharge scenario from 2020 to 2100. Maximum and average ratios of base case to increased recharge case for uranium and nitrate concentrations at both well locations.

4.4. Cap-Failure Scenarios

In the cap-failure scenarios, pH is always lower than the base case across +10% ~ +50% recharge rates (Figure 10a). At the source-zone well, these pH values dip below 3.5 in 2030, rebound to 4.0 after 2045, and then slightly increase to 4.3 by the end of the simulation. The +50% cap-failure scenario has the highest pH value compared to the +10 ~ +40% cap-failure cases. Nitrate concentrations spike and increase one order of magnitude in 2030, then decrease to the same level as the base case in 2050 (Figure 10b). The pattern of tritium and uranium breakthrough curves (Figure 10 c-d) look very similar to nitrate. Among the breakthrough curves of nitrate, tritium, and uranium across all cap-failure scenarios, the +50% cap-failure scenario simulates the earliest peak, while the +20% scenario simulates the highest peak. At the downgradient well, pH values at all cap-failure scenarios increase with the base case in the first ten years, then decrease around 2035 and remain lower than the base case (Figure 10e). pH values only decrease from 5.5 to 5.0 in the smaller +10 ~ +20% recharge rates. However, they decrease significantly with greater recharge rates (+30% ~ +50%) in those cap-failure scenarios. The breakthrough curves of pH increase in the first ten years after 2020,

https://doi.org/10.5194/hess-2021-338
Preprint. Discussion started: 2 August 2021

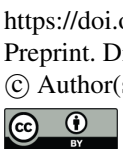

Hydrology and Earth System Sciences
Discussions
Open Access
EGU

dip to 3.6 around 2040, and then slightly increase, but require several decades to rebound to the same pH level as in 2020. Compared to the nitrate concentration breakthrough curves at the source-zone well (Figure 10b), the peaks at the downgradient well are simulated in 2040 with a 10-year delay (Figure 10f). The nitrate concentrations in those greater (+30% ~ 50%) recharge rates occur earlier and are higher than in the smaller (+10% ~ 20%) recharge rates. The tritium concentration shows similar peaks as nitrate, but the earliest peak with +50% cap failure has the highest values, and the later peaks with smaller (+10% ~ 20%) recharge rates will be lower because of tritium radioactive decay (Figure 10g). Uranium concentration breakthrough curves show similar behaviors to nitrate in both wells (Figure 10bd and fh).

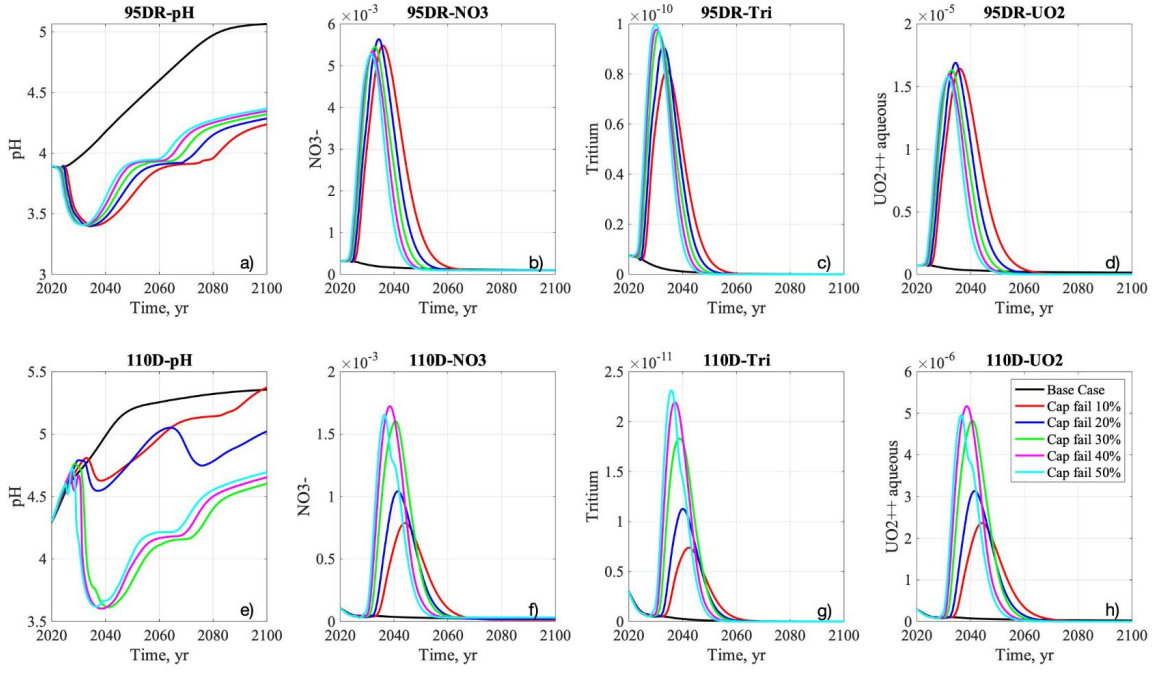

Figure 10. Breakthrough curves of pH, aqueous uranium, tritium, and nitrate at the source-zone well (a-d) and downgradient well (e-h) in the base case and cap-failure scenarios from 2020 to 2100.

Kd breakthrough curves are highly correlated with pH at both monitoring wells (Figure 10ae), Kd decreases by 2035 and 2040 at both wells, respectively, returns to the 2020 level around 2050, then keeps increasing until 2100. At the source-zone well, Kd values decrease and rebound fastest in the +50% recharge case, and the smallest +10% recharge rate case shows a similar trend but is delayed by nearly 10 years (Figure 11a). At the downgradient well, the Kd breakthrough curves at higher recharge cases (+30% ~ +50%) are more closely correlated with pH and decrease around 2040, while smaller recharge cases (+10% ~ +20%) are more similar to the base case (Figure 11d). A turning point occurs in 2040, when the +30% case switches

https://doi.org/10.5194/hess-2021-338
Preprint. Discussion started: 2 August 2021

Hydrology and Earth System Sciences
Discussions
Open Access
EGU

places with the +50% case and has the lowest Kd value until 2100, similar to the behavior of aqueous uranium breakthrough curves in 2040 (Figure 10h). When comparing Figure 11d and Figure 10e, it is clear that although pH is not the highest in the +20% cap-failure scenario, after 2070, that scenario has the highest Kd value and more adsorption. In cap failure scenarios, the maximum and average uranium concentration ratios are consistently greater than nitrate in both wells, and follow the same trend with increasing recharge rates (Figure 11b-c, e-f). Both ratios of uranium and nitrate maximum and average concentration are one order of magnitude greater than the base case. The maximum concentrations of uranium and nitrate are observed in 2030 and 2040 at the source-zone well and downgradient well, respectively (Figure 10bf), although it is difficult to tell the difference from the breakthrough curves because of the magnitude of peak concentrations. The uranium and nitrate maximum concentration ratios are highest in the 20% cap-failure scenarios (Figure 11b), and decrease with greater increasing recharge rate. The ratios of uranium average concentrations against base case are also persistently higher than nitrate in the long term throughout 2100, and decrease with greater recharge rate (Figure 11c). At the downgradient well, the maximum concentration ratio against the base case generally increases with greater recharge rate, and is the largest in the +40% recharge case (Figure 11e). The average concentration ratio increases with the smaller (+10% ~ +30%) recharge rates, then decreases with the greater (+40% ~ +50%) recharge rates (Figure 11f).

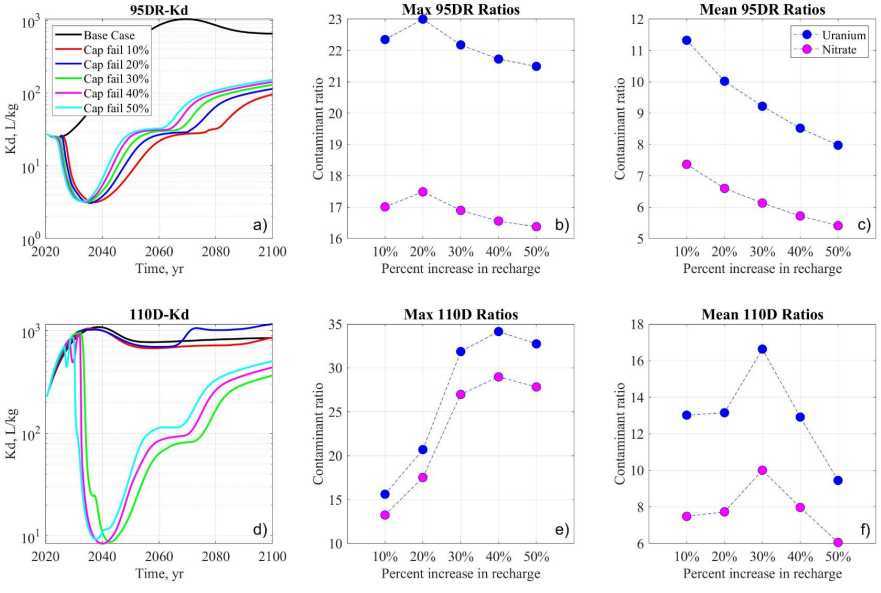

Figure 11 : Breakthrough curves for Kd at the source-zone well (a-c) and the downgradient well (d-f) for the increasing recharge scenario from 2020 to 2100. Maximum and average ratios of base case to increased recharge case for uranium and nitrate concentrations at both well locations.

https://doi.org/10.5194/hess-2021-338
Preprint. Discussion started: 2 August 2021


Hydrology and Earth System Sciences
Discussions

4.5. Climate Model Scenarios

Recharge rates are calculated by subtracting evapotranspiration from precipitation (precipitation - evapotranspiration) in the four CMIP5 climate projection scenarios. The highest greenhouse gas concentration pathway RCP8.5 scenario has the maximum simulated precipitation and evapotranspiration. However, the differences in recharge rate are small across those four scenarios as both precipitation and evapotranspiration increase in the projection (Figure 3). Therefore, the concentration breakthrough curves are similar under those climate scenarios. The average recharge rate in those scenarios is around 8.0e-6 kg-water/m^2/sec (0.253 m/yr), or approximately 1.68 times higher than the base case. In general, simulated contaminant concentrations in those climate scenarios are lower than the base case due to dilution effects with greater recharge rate, except that pH values are also lower than the base case (Figure 12). The breakthrough curves decrease faster before 2020 (not shown in Figure 12) and reach background concentration sooner than the base case.

At the source-zone well, the pH breakthrough curve gradually rebounds from 4.0 to 4.5 by the end of the simulation (Figure 12a). Both nitrate and uranium concentrations show annual variability after 2020, as recharge rates are changing annually (Figure 12bd). Specifically, nitrate breakthrough curves (Figure 12b) become steady state sooner than the uranium, as nitrate background concentration is higher. The oscillation is hardly observed in tritium concentration breakthrough curves, as it decreases faster due to decay. At the downgradient well, pH values across climate scenarios are consistently lower than the base case with annual variability (Figure 12e). Compared to the results at the source-zone well, the nitrate concentrations at the downgradient well (Figure 12f) are lower than the background level with greater annual variability, and become steady state a few years later. The tritium concentration becomes extremely low below 1e-15 (Figure 12g), while uranium concentrations return to background level after 2030 (Figure 12h).

https://doi.org/10.5194/hess-2021-338
Preprint. Discussion started: 2 August 2021

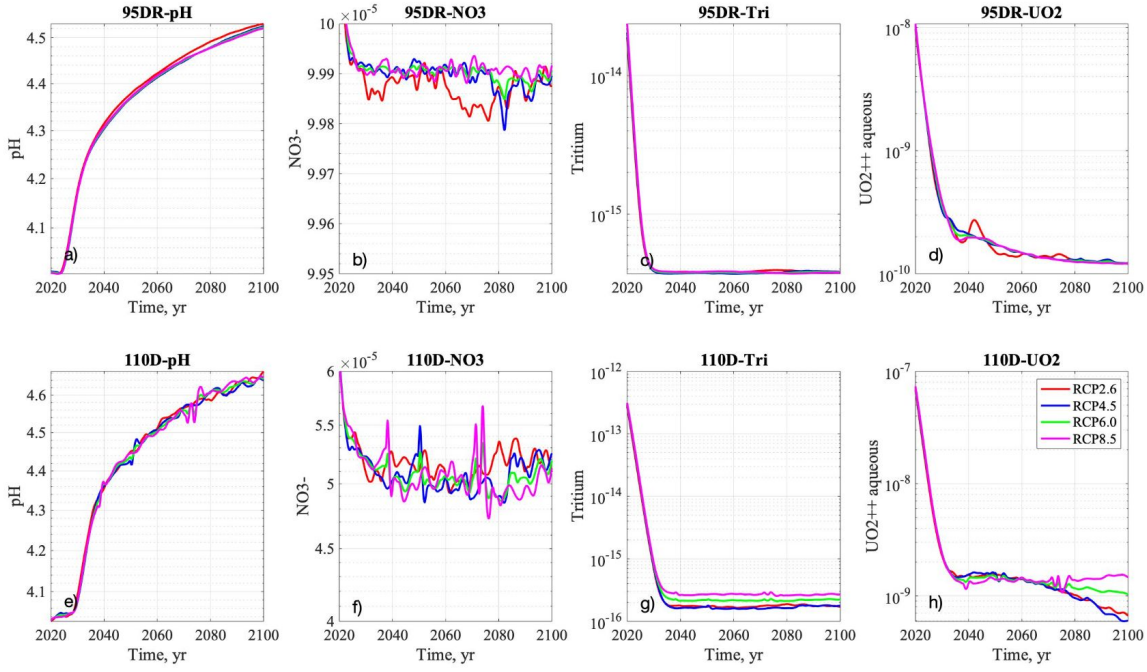

Figure 12. Breakthrough curves of pH, nitrate, tritium, and aqueous uranium at the source-zone well (a-d) and downgradient well (e-h) in the climate scenarios from 2020 to 2100.

5. DISCUSSION

A balance between dilution and remobilization is a key factor determining the contaminant concentration depending on recharge rates, as discussed in Libera et al. (2019). Generally in the increasing recharge scenarios, contaminant concentrations decrease first due to dilution, and then increase because the mobilized contaminants migrate from the source zones to the wells. The highest recharge scenario has the earliest and highest peak in contaminant concentrations due to a stronger remobilization effect, but it has the lowest concentrations and highest pH later due to dilution. Additionally, in the later period, the increasing recharge again causes dilution due to flushing, resulting in a concentration level below the base case. Because of long-term dilution, the aqueous uranium concentration in greater increasing recharge scenarios is even lower than the base case at the source-zone well after 2035. The relationships between concentrations and recharge are nonlinear and nonmonotonic, depending on different times and locations. Changing recharge rate has less impact at the downgradient well where the spikes are delayed for approximately 10 years since its location is further from the seepage basin, and it takes time for the remobilized plume to reach it. The breakthrough curves of smaller (+10% ~ +30%) increasing recharge scenarios are similar to those of the base

https://doi.org/10.5194/hess-2021-338
Preprint. Discussion started: 2 August 2021


Hydrology and Earth System Sciences
Discussions

570 case, with slight dilution effects throughout 2100, while concentration spikes due to remobilization in 2040 are observed with the larger (+40 ~ +50%) increasing recharge scenarios (Figure 6eh).

In the early stage of decreasing recharge scenarios, contaminant concentrations increase
575 because of diminished flushing and a low flow rate of clean groundwater. Later in the simulation period, contaminant concentrations decrease significantly in the greater decreasing recharge scenarios, when the groundwater table declines and isolates the residual contaminants in the vadose zone. This was not observed in the previous tritium simulation (Libera et al., 2019) because of tritium's radioactive decay. In general, this means that decreasing precipitation and
580 droughts are effective in sequestering contaminants in the vadose zone. At the same time, it implies less flushing and an increase in residence time of the contaminants at the site. The uncontaminated groundwater from the upgradient also migrates more slowly in the aquifer. The larger volume of residual contaminants could potentially increase risk, particularly considering extreme precipitation events, which are projected to happen more frequently in many climate
585 models (USGCRP, 2017). Also, when there is a drought, there is more interest in groundwater resources, which could lead to increased pumping in the contaminated aquifer. Although such pumping activities are strictly regulated at our study site, such trade-offs require attention at other sites.

590 To investigate the impact on reactive species such as uranium, we compared reactive (uranium) and nonreactive (nitrate) concentration ratios to assess the impacts of reaction and sorption. We originally hypothesized that increasing recharge would decrease reactive species concentration further, since increasing the volume of water in the domain would increase pH, which limits the mobility of uranium. However, Figure 7 shows that the uranium-concentration
595 ratios compared to the base case increase more significantly than the nitrate concentrations. This is because the remobilization occurs when the pH is still low, and also because remobilization happens to both uranium and protons (Figure 6). In addition, the amount of the residual contaminants is larger for uranium than nitrate due to sorption. Later in the simulation period, the uranium average concentrations are lower than for nitrate and decrease with greater
600 recharge scenarios, because increasing pH, due to long-term dilution by additional recharge, immobilizes uranium.

In cap-failure scenarios, sorption of uranium is reduced with increasing infiltration, because Kd is sensitive to lower pH due to remobilization through the basin. At the downgradient well, the
605 greater recharge cases (+30% ~ +50%) have a more closely correlated Kd and pH, and have a higher aqueous uranium concentration, than the lower recharge scenarios. In our scenarios, there is a clear change in the balance of aqueous and sorbed uranium concentration in the transition from +20% to +30% recharge, where the system's sorption in the downgradient fundamentally changes. The cap-failure cases indicate that changing recharge and cap-failure
610 levels can trigger dramatic changes in pH and sorption. Consistent with Libera et al. (2019), this study confirms the importance of cap or surface barriers to limit the impacts of cap failure under extreme climate regimes.

https://doi.org/10.5194/hess-2021-338
Preprint. Discussion started: 2 August 2021


Hydrology and Earth System Sciences
Discussions

Adsorption and ion exchange in kaolinite and goethite retards pH and uranium concentration fronts (Bea et al., 2013). Adsorption/exchange sites are limited and saturated by the lower pH and higher uranium concentration loading, and eventually reach steady state in 2100. Overall in our scenarios, the change in recharge has a similar impact on uranium and nonreactive species, which is largely attributed to pH buffering due to mineral precipitation. The increase in pH due to dilution encourages the precipitation of kaolinite, but the precipitation reaction of kaolinite produces H^+ ions, which then decreases pH. At low pH, the hydroxyl groups on the octahedral structures of aluminosilicates like kaolinite become protonated, effectively creating a net positive charge on the mineral. This means that uranium cannot sorb to the clay and is therefore mobile in the system. Previous experimental (Dong et al. 2012) and modeling (Arora et al., 2018) studies also reaffirmed that percent U(VI) sorption is greater with a higher, neutralized pH, because U(VI) and H^+ are competing in sorption. This is the process of dissolution and precipitation of kaolinite:

$$Al_2Si_2O_5(OH)_4 + 6H^+ \leftrightarrow 2Al^{3+} + 2SiO_2 + 5H_2O$$

A similar reaction occurs with gibbsite. While it was thought to be irrelevant for this particular study area within F-Area, some recharge scenarios suggest that there could be more gibbsite formation than previously thought. Dong et al. (2012) showed that there was an insignificant weight percent or volume fraction of gibbsite at F-Area, since it only forms at pH>5.4. However, in the decreasing recharge scenarios, all the recharge cases at the downgradient well have a pH between 5.4 and 7 after 2070, and pH at the two greater recharge cases at the source-zone well also surpass 5.4. Decreasing recharge would likely trigger the formation of gibbsite, which could increase pH buffering. Additionally, according to Bea et al. (2013), this mechanism, as well as cation exchange and adsorption processes on kaolinite and goethite, explain some buffering of pH. The pH buffering effect is the major mechanism for pH remaining low for an extended period of time in climate resilience studies with reactive transport modeling.

In addition to understanding the impact of a range of recharge scenarios, this study has established a pipeline to use the CMIP5 climate model projections as input to the hydrology and reactive transport modeling simulations. Although increasing precipitation is projected over time, we found that the increasing ET associated with temperature can reduce the recharge rates. We found that, compared to the base case and hypothetical scenarios, the CMIP5 climate data projects a small increase or no change of recharge rate over time, indicating that the changing climate has minor effects on the contamination plume and breakthrough curves in our study site. This is similar to the behaviors observed in the increasing precipitation scenarios in Figure 6: that smaller recharge increases have little impact on the concentration breakthrough curves, because the increasing recharge is below the threshold that may cause significant remobilization. Contaminant migration is more controlled by the transport process. The reactive transport modeling with CMIP5 projection also reveals the sensitivity of recharge rates, and indicates that the uncertainty associated with simulated ET and precipitation could significantly affect the assessment of waste disposal and contaminant transport.

https://doi.org/10.5194/hess-2021-338
Preprint. Discussion started: 2 August 2021


Hydrology and Earth System Sciences
Discussions

4. CONCLUSION

The climate resilience of residual contamination at the SRS F-Area waste disposal site throughout the projection period from 2020 to 2100 is investigated in this study. Groundwater flow, mineral reactions, surface complexation sorption, and ion-exchange processes are simulated by the Amanzi and PFLOTRAN flow and reactive transport model. We illustrate four scenarios characterized by a range of variable recharge values: (1) increasing recharge after 2020, (2) decreasing recharge after 2020, (3) cap failure and constant positive recharge shift, and (4) recharge rate under different RCP scenarios from the CMIP5 climate model projection. Although exaggerated in the first three cases, this systematic study using changing recharge rates was useful in identifying the phased impacts of increasing or decreasing recharge rates, as well as the difference between the reactive and nonreactive species. Plume distribution and breakthrough curves of chemical species are evaluated to assess the impacts of changing recharge rate and flow conditions. The ratios of maximum and average reactive and nonreactive species concentrations between scenarios and base case are used to understand how climate change affects the adsorption and ion exchange of residual contaminants in the subsurface domain. Furthermore, Kd breakthrough curves are evaluated to understand the pH effects on sorption with different recharge rates in those scenarios.

With increasing recharge rates, pH decreases and residual contaminant concentrations increase, because of the remobilization of protons and reactive species. The impact on uranium or pH-dependent species is the same as nonreactive contaminants. Kd values are correlated with pH and behave differently when changing recharge rates beyond certain thresholds. In most cases, uranium-maximum concentration ratios against the base case are higher than the nitrate concentration ratios, owing to remobilization, while the uranium concentration breakthrough curves in the later period depend on long-term flow conditions. The results of cap-failure scenarios suggest that reactive transport modeling and analysis of pH effects on reactive species are important for the risk assessment of such engineering failures.

Our results highlight that climate change impacts may not be intuitive, and must be analyzed quantitatively by models. ET projection has great uncertainty, but is particularly important in determining the recharge rates in reactive transport modeling for climate resilience studies. Reactive transport models which consider pH dependency for reactive species are essential for analyzing the impacts of pH with changing recharge rates. Although this study is focused on one site, we developed the pipeline to use climate projection datasets in reactive transport modeling and thereby demonstrated the capability for assessing climate change impacts on waste disposal sites. We expect that our approach and insight are transferable to other sites that have large amounts of residual contaminants in the vadose zones or in the groundwater.

ACKNOWLEDGMENTS

https://doi.org/10.5194/hess-2021-338
Preprint. Discussion started: 2 August 2021

This study is supported by the Department of Energy, Office of Environmental Management Technology Development Program under ALTEMIS - Advanced Long-Term Environmental Monitoring Systems project, the Department of Energy's Savannah River Area Completion project, as well as by the Office of Science, Biological and Environmental Sciences under Scientific under the Scientific Focus Area. This research used resources of the National Energy Research Scientific Computing Center (NERSC), a U.S. Department of Energy Office of Science User Facility located at Lawrence Berkeley National Laboratory, operated under Contract No. DE-AC02-05CH11231. This research also used the Lawrencium computational cluster resource provided by the IT Division at the Lawrence Berkeley National Laboratory (Supported by the Director, Office of Science, Office of Basic Energy Sciences, of the U.S. Department of Energy under Contract No. DE-AC02-05CH11231).

REFERENCE

Abtew, W., & Melesse, A. (2013). Climate change and evapotranspiration. In Evaporation and evapotranspiration (pp. 197-202). Springer, Dordrecht.

Arora, B., Davis, J. A., Spycher, N. F., Dong, W., & Wainwright, H. M. (2018). Comparison of Electrostatic and Non-Electrostatic Models for U (VI) Sorption on Aquifer Sediments. Groundwater, 56(1), 73-86.

Bea, S. A., Wainwright, H., Spycher, N., Faybishenko, B., Hubbard, S. S., & Denham, M. E. (2013). Identifying key controls on the behavior of an acidic-U (VI) plume in the Savannah River Site using reactive transport modeling. Journal of contaminant hydrology, 151, 34-54.

Bloomfield, J. P., Williams, R. J., Gooddy, D. C., Cape, J. N., & Guha, P. M. (2006). Impacts of climate change on the fate and behaviour of pesticides in surface and groundwater—a UK perspective. Science of the total Environment, 369(1-3), 163-177.

Curtis, G. P., Davis, J. A., & Naftz, D. L. (2006). Simulation of reactive transport of uranium (VI) in groundwater with variable chemical conditions. Water Resources Research, 42(4).

Darracq, A., Greffe, F., Hannerz, F., Destouni, G., & Cvetkovic, V. (2005). Nutrient transport scenarios in a changing Stockholm and Mälaren valley region, Sweden. Water Science and Technology, 51(3-4), 31-38.

Davis, J. A., Meece, D. E., Kohler, M., & Curtis, G. P. (2004). Approaches to surface complexation modeling of uranium (VI) adsorption on aquifer sediments. Geochimica et Cosmochimica Acta, 68(18), 3621-3641.

Denham, M., Eddy-Dilek, C., 2017. Influences on effective decay rates of radionuclides in groundwater: F-Area Seepage Basins, Savannah River site. In: WM2017 Conf. Phoenix, Arizona, USA.

Denham, M. E., Amidon, M. B., Wainwright, H. M., Dafflon, B., Ajo-Franklin, J., & Eddy-Dilek, C. A. (2020). Improving Long-term Monitoring of Contaminated Groundwater at Sites where Attenuation-based Remedies are Deployed. Environmental Management, 66(6), 1142-1161.

Destouni, G., & Darracq, A. (2009). Nutrient cycling and N2O emissions in a changing climate: the subsurface water system role. Environmental Research Letters, 4(3), 035008.

https://doi.org/10.5194/hess-2021-338
Preprint. Discussion started: 2 August 2021

Dong, W., Tokunaga, T. K., Davis, J. A., & Wan, J. (2012). Uranium (VI) adsorption and surface complexation modeling onto background sediments from the F-Area Savannah River Site. Environmental science & technology, 46(3), 1565-1571.

Fenimore, J.W., and Horton, J.H.Rating history and environmental effects of seepage basins in the chemical separations areas of the Savannah River Plant. USAEC report, DPST-72-548. USAEC, Washington, DC. 1972

Flach, G. P., Crisman, S. A., & Molz III, F. J. (2004). Comparison of single-domain and dual-domain subsurface transport models. Ground Water, 42(6/7), 815.

Futter, M. N., Helliwell, R. C., Hutchins, M., & Aherne, J. (2009). Modelling the effects of changing climate and nitrogen deposition on nitrate dynamics in a Scottish mountain catchment. Hydrology Research, 40(2-3), 153-166.

Gellens, D., & Roulin, E. (1998). Streamflow response of Belgian catchments to IPCC climate change scenarios. Journal of hydrology, 210(1-4), 242-258.

Green, T. R., Taniguchi, M., Kooi, H., Gurdak, J. J., Allen, D. M., Hiscock, K. M., ... & Aureli, A. (2011). Beneath the surface of global change: Impacts of climate change on groundwater. Journal of Hydrology, 405(3-4), 532-560.

Hammond, G. E., Lichtner, P. C., & Rockhold, M. L. (2011). Stochastic simulation of uranium migration at the Hanford 300 Area. Journal of Contaminant Hydrology, 120, 115-128.

Johnson, J. N., & Molins, S. (2015). Alquimia: Exposing mature biogeochemistry capabilities for easier benchmarking and development of next-generation subsurface codes. AGUFM, 2015, B43B-0542.

Lambert, F. H., Stine, A. R., Krakauer, N. Y., & Chiang, J. C. (2008). How much will precipitation increase with global warming?. EOS, Transactions American Geophysical Union, 89(21), 193-194.

Li, R., & Merchant, J. W. (2013). Modeling vulnerability of groundwater to pollution under future scenarios of climate change and biofuels-related land use change: A case study in North Dakota, USA. Science of the total environment, 447, 32-45.

Libera, A., de Barros, F. P., Faybishenko, B., Eddy-Dilek, C., Denham, M., Lipnikov, K., ... & Wainwright, H. (2019). Climate change impact on residual contaminants under sustainable remediation. Journal of contaminant hydrology, 226, 103518.

Lichtner, P. C., Hammond, G. E., Lu, C., Karra, S., Bisht, G., Andre, B., ... & Kumar, J. (2015). PFLOTRAN user manual: A massively parallel reactive flow and transport model for describing surface and subsurface processes (No. LA-UR-15-20403). Los Alamos National Lab.(LANL), Los Alamos, NM (United States); Sandia National Lab.(SNL-NM), Albuquerque, NM (United States); Lawrence Berkeley National Lab.(LBNL), Berkeley, CA (United States); Oak Ridge National Lab.(ORNL), Oak Ridge, TN (United States); OFM Research, Redmond, WA (United States).

Maco, B., Bardos, P., Coulon, F., Erickson-Mulanax, E., Hansen, L. J., Harclerode, M., ... & Wick, W. D. (2018). Resilient remediation: Addressing extreme weather and climate change, creating community value. Remediation Journal, 29(1), 7-18.

Middelkoop, H., Daamen, K., Gellens, D., Grabs, W., Kwadijk, J. C., Lang, H., ... & Wilke, K. (2001). Impact of climate change on hydrological regimes and water resources management in the Rhine basin. Climatic change, 49(1-2), 105-128.

https://doi.org/10.5194/hess-2021-338
Preprint. Discussion started: 2 August 2021


Hydrology and Earth System Sciences
Discussions

Milly, P. C., & Dunne, K. A. (2016). Potential evapotranspiration and continental drying. Nature Climate Change, 6(10), 946-949.

Moulton, J. D., Molins, S., Johnson, J. N., Coon, E., Lipnikov, K., Day, M., & Barker, E. (2014). Amanzi: An Open-Source Multi-process Simulator for Environmental Applications. AGUFM, 2014, H51K-0758.

Olesen, J. E., Carter, T. R., Diaz-Ambrona, C. H., Fronzek, S., Heidmann, T., Hickler, T., ... & Quemada, M. (2007). Uncertainties in projected impacts of climate change on European agriculture and terrestrial ecosystems based on scenarios from regional climate models. Climatic Change, 81(1), 123-143.

Park, M. J., Park, J. Y., Shin, H. J., Lee, M. S., Park, G. A., Jung, I. K., & Kim, S. J. (2010). Projection of future climate change impacts on nonpoint source pollution loads for a forest dominant dam watershed by reflecting future vegetation canopy in a Soil and Water Assessment Tool model. Water Science and Technology, 61(8), 1975-1986.

Pfister, L., Kwadijk, J., Musy, A., Bronstert, A., & Hoffmann, L. (2004). Climate change, land use change and runoff prediction in the Rhine–Meuse basins. River research and applications, 20(3), 229-241.

Rahmstorf, S., & Coumou, D. (2011). Increase of extreme events in a warming world. Proceedings of the National Academy of Sciences, 108(44), 17905-17909.

Sassen, D. S., Hubbard, S. S., Bea, S. A., Chen, J., Spycher, N., & Denham, M. E. (2012). Reactive facies: An approach for parameterizing field-scale reactive transport models using geophysical methods. Water Resources Research, 48(10).

Savannah River Nuclear Solution, (2021). Annual Corrective Action Report for the F-Area Hazardous Waste Management Facility, the H-Area Hazardous Waste Management Facility, and the Mixed Waste Management Facility (U), SRNS-RP-2021-00513.

Schiedek, D., Sundelin, B., Readman, J. W., & Macdonald, R. W. (2007). Interactions between climate change and contaminants. Marine pollution bulletin, 54(12), 1845-1856.

Sherman, D. M., Peacock, C. L., & Hubbard, C. G. (2008). Surface complexation of U (VI) on goethite (α-FeOOH). Geochimica et Cosmochimica Acta, 72(2), 298-310.

Serkiz, S. M., Johnson, W. H., Wile, L. J., & Clark, S. B. (2007). Environmental availability of uranium in an acidic plume at the Savannah River Site. Vadose Zone Journal, 6(2), 354-362.

Sjøeng, A. M. S., Kaste, Ø., & Wright, R. F. (2009). Modelling future NO3 leaching from an upland headwater catchment in SW Norway using the MAGIC model: II. Simulation of future nitrate leaching given scenarios of climate change and nitrogen deposition. Hydrology Research, 40(2-3), 217-233.

Taylor, K. E., Stouffer, R. J., & Meehl, G. A. (2012). An overview of CMIP5 and the experiment design. Bulletin of the American meteorological Society, 93(4), 485-498.

USGCRP, 2017: Climate Science Special Report: Fourth National Climate Assessment, Volume I [Wuebbles, D.J., D.W. Fahey, K.A. Hibbard, D.J. Dokken, B.C. Stewart, and T.K. Maycock (eds.)]. U.S. Global Change Research Program, Washington, DC, USA, 470 pp., doi: 10.7930/J0J964J6.

Visser, A., Kroes, J., van Vliet, M. T., Blenkinsop, S., Fowler, H. J., & Broers, H. P. (2012). Climate change impacts on the leaching of a heavy metal contamination in a small lowland catchment. Journal of contaminant hydrology, 127(1-4), 47-64.

https://doi.org/10.5194/hess-2021-338
Preprint. Discussion started: 2 August 2021


Hydrology and Earth System Sciences
Discussions

Van Bokhoven, A. J. (2006). The impact of climate change on the water quality of the Rhine river.

Van Vliet, M. T. H., & Zwolsman, J. J. G. (2008). Impact of summer droughts on the water quality of the Meuse river. Journal of Hydrology, 353(1-2), 1-17.

Wainwright, H. M., Chen, J., Sassen, D. S., & Hubbard, S. S. (2014). Bayesian hierarchical approach and geophysical data sets for estimation of reactive facies over plume scales. Water Resources Research, 50(6), 4564-4584.

Wainwright, H. M., Molins, S., Davis, J., Arora, B., Faybishenko, B., Krishnan, H., ... & Moulton, D. (2015, March). Using ASCEM modeling and visualization to inform stakeholders of contaminant plume evolution and remediation efficacy at F-basin Savannah River, SC. In WM2015 Conference. Phoenix, Arizona (pp. 1-14).

Wainwright, H., Faybishenko, B., Molins, S., Davis, J., Arora, B., Pau, G., ... & Moulton, D. (2016). Effective Long-term Monitoring Strategies by Integrating Reactive Transport Models with In situ Geochemical Measurements–16212. In WM2016 Conf (pp. 1-15).

Whitehead, P. G., Wilby, R. L., Battarbee, R. W., Kernan, M., & Wade, A. J. (2009). A review of the potential impacts of climate change on surface water quality. Hydrological sciences journal, 54(1), 101-123.

Wilby, R. L., Whitehead, P. G., Wade, A. J., Butterfield, D., Davis, R. J., & Watts, G. (2006). Integrated modelling of climate change impacts on water resources and quality in a lowland catchment: River Kennet, UK. Journal of hydrology, 330(1-2), 204-220.